MATERIAL EJECTA IN A DISTURBED SOLAR FILAMENT

M. A. RAADU

Royal Institute of Technology, Department of Plasma Physics, S-100 44 Stockholm, Sweden

J. M. MALHERBE, B. SCHMIEDER, and P. MEIN

Observatoire de Paris, Section de Meudon, DASOP – UA 326, 92195 Meudon, Principal Cedex, France

(Received 22 July; in revised form 9 February, 1987)

Abstract. Hα observations, using the Multichannel Subtractive Double Pass (MSDP) spectrograph operating on the Meudon Solar Tower, have been made of an active region filament which undergoes a 'disparition brusque'. The period of observation was from 10 : 45 to 13 : 30 UT on 22 June, 1981. Velocity and intensity fluctuations in Hα were measured. The proper motions of ejecta were followed allowing their trajectories and vector velocities to be determined. To model the dynamics of ejecta several models using thermal or magnetic driving forces are compared. The most promising model explains the motion as the consequence of magnetic stresses acting on an isolated magnetized plasmoïd in a diverging flux tube.

1. Introduction

Quiescent prominences, which appear as filaments on the solar disk, are long sheet-like structures of cool matter suspended in the solar corona. Generally, they develop slowly and persist for several months. From time to time they may, however, be strongly disturbed and disappear (as an Hα-structure) as the result of what is termed a 'disparition brusque' (DB). The disappearance may be caused by heating or by dynamical processes (Mouradian *et al.*, 1986). During a thermal DB heating raises the temperature of the prominence material so that it is no longer visible in Hα (Malherbe *et al.*, 1983a). During a dynamical DB the activated prominence becomes strongly unstable and material is ejected at high velocity. The dynamics of ejected matter as the consequence of such a filament disturbance is the subject of this paper. DB's may occur for both old quiescent prominences distant from active regions and also for active region filaments. Active region DB's are often associated with flares which may act as a trigger providing a large amplitude perturbation. An intrinsically stable prominence may be expected to respond by oscillating. Kleczek and Kuperus (1969) develop a model for horizontal oscillations in prominences which agrees well with observations. Current sheet models such as that of Kuperus and Raadu (Raadu and Kuperus, 1973; Kuperus and Raadu, 1974; Raadu, 1979) imply magnetically stored energy which may be released as kinetic energy. Van Tend and Kuperus (1978) have shown how instabilities can develop for currents supporting prominence material. Priest and Heyvaerts (1974) argue that the development of plasma turbulence can destabilise a current sheet containing prominence material. Rust (1976) presents observational evidence that the rapid emergence of new magnetic flux may be a trigger for filament activation and flaring. Emerging flux can be expected to lead to current sheet formation in the corona. Simon *et al.* (1984) suggest that the emergence of new magnetic flux and associated recon-

Solar Physics **109** (1987) 59–79.

nection processes may be the underlying cause of the preflare activity which they have observed in a solar prominence. In the present paper we will not consider the total 'disparition brusque' phenomenon. Instead, we will consider the local dynamics of ejecta produced in a DB. Our investigation should, however, provide further clues to the large scale properties of DB's.

Observations were made of the velocity fields and intensity fluctuations in Hα during a DB. The proper motion of isolated condensations within the filament were followed and in combination with the Doppler shift measurements, it was possible to deduce the vector components of the velocity and the trajectory of the moving condensations (cf. Malherbe *et al.*, 1983b).

We examine both pressure and magnetic driving mechanisms for the mass motions. Steady siphon flows of the type used by Meyer and Schmidt (1968) are considered. A piston model in which a blob of cold material is accelerated by the pressure of hot coronal plasma (cf. the 'coronal bullets' of Karpen *et al.*, 1982) is also tested against the observations. Possible magnetic mechanisms investigated here are the expansion of a 'magnetic spring' and acceleration of a magnetized plasmoïd. The latter model seems most promising in the present case.

2. Observations and Data Reduction

2.1. Instruments

A large filament (11 arc sec long), located north-west of NOAA (Boulder) active region 3170 (N 15, E45) was observed during 3 days on 21, 22, 23 June, 1981 by the Hα spectroheliograph and the 3 wavelength heliograph (Hα ± 0.75 Å), at Meudon Observatory. It was also observed on 22 June, 1981 by the Multichannel Subtractive Double Pass (MSDP) spectrograph operating at the Meudon solar tower (Mein, 1977) and by the radioheliograph (169 MHz) (Radioheliograph Group, 1983) and by the numerical multichannel radiospectrograph (152 to 468 MHz) operating at Nançay (Dumas *et al.*, 1982).

2.2. Morphological evolution of the filament

The observed filament consists of two different sections noted (a) and (b) on the Hα spectroheliogram obtained on 22 June, 1981 (Figure 1(a)). The MSDP observations show that section (a) is disappearing, the southern part first, on the same day between 10 : 45 to 13 : 30 UT while section (b) is stable. On the next day, the section (a) has completely disappeared (Figure 1(b)).

The radio data show that type I storms and type III bursts occur between 07 : 46 to 13 : 52 UT during the 'disparition brusque' of section (a) but they are located in the vicinity of section (b). These events precede a large flare located in the active center between the two sunspots at 14 : 45 UT.

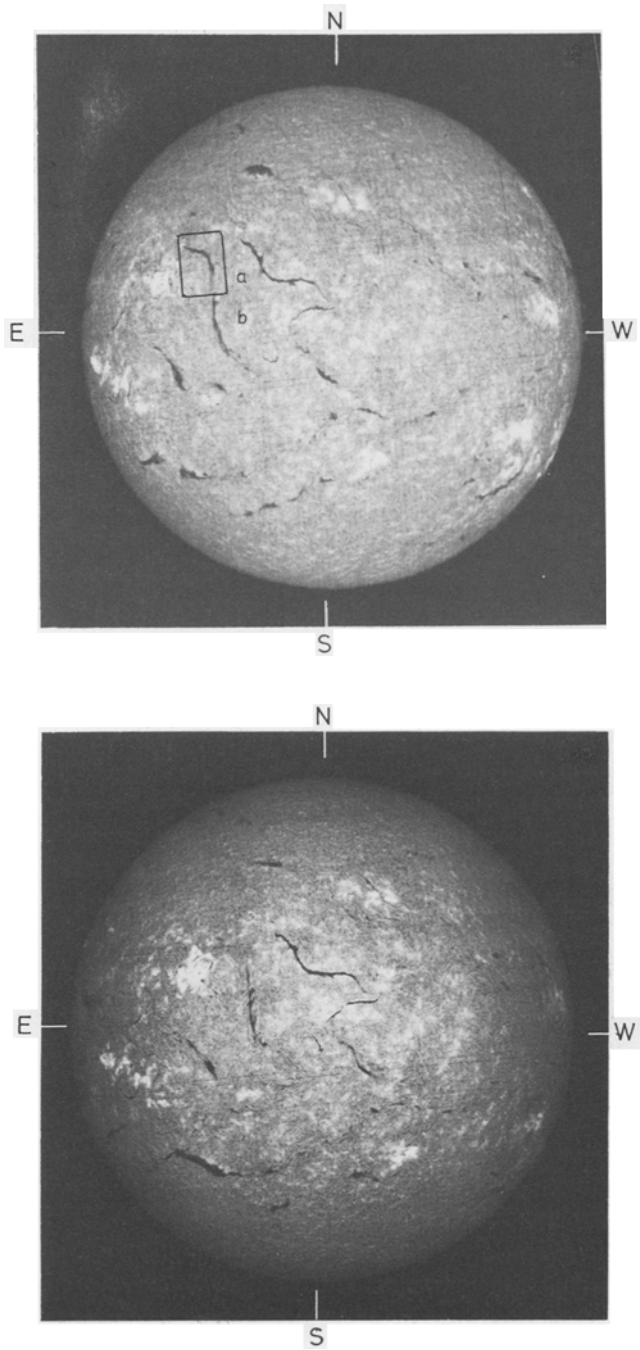

Fig. 1. Spectroheliograms in Hα line (Meudon): 22 June, 1981 (above), 23 June, 1981 (below). The two components (a) and (b) of the disappearing filament are indicated in the upper spectroheliogram. Part (a) is no more visible on June 23.

2.3. MSDP TECHNIQUE

The MSDP provided nine simultaneous intensity images in the Hα profile with a spatial resolution of the order of 1″. Because of the nature of the instrument the position in the line profile is a function of position in the field of view. These data allow us to construct a line profile for each point in the 2D field of view. To reduce the data we first construct a mean profile $I_0(\lambda)$ over the quiet Sun regions of each elementary field of view of the MSDP (1′ × 8′). For the mean profiles and the profile of each point $I(\lambda)$, we then find the points in the profiles where the half width is 0.3 Å. The wavelength shift between each ± 0.3 Å chord is used to calculate the radial velocity V, and the intensity shift between the two chords determines the relative intensity ΔI (lambda-meter technique). A global field of view of 5′ × 8′ is obtained by a juxtaposition of five elementary fields observed within 1 mn in time.

2.4. THE DB OF THE FILAMENT ON 22 JUNE, 1981

Figure 2 shows maps of MSDP intensity fluctuations and radial velocities in Hα ± 0.3 Å at 3 different times covering the DB of section (a) during the disappearance, which begins in the southern part; slow upward motions are observed inside the filament ($V < 6$ km s^{-1}) while slow downward motions occur at its edges. The lifetime of the upward motions is large, about 1 hr; that of downward motions is short, about 5 mn.

The asymmetry of the Hα profiles in the filament (Figure 3) with more absorption in the blue wing than in the red wing, indicates thin threads, with high upward radial velocities (material ejecta).

3. Dynamics of Material Ejecta

3.1. CONTRAST INTERPRETED USING BECKERS' CLOUD MODEL

In order to find the values of the upward radial velocities of the filament we interpret the Hα contrasts ($C = \Delta I/I_0(\lambda)$ where $\Delta I(\lambda) = I(\lambda) - I_0(\lambda)$) using Beckers' (1964) cloud model as we have done previously for surges (Schmieder *et al.*, 1983, 1984).

If the source function S is assumed to be constant in the cloud, its contrast is given by

$$C(\Delta\lambda) = \left[\frac{S}{I_0} - 1\right][1 - \exp(-t(\Delta\lambda))],$$

where $t(\Delta\lambda)$ is the optical thickness of the cloud:

$$t(\Delta\lambda) = t_0 \exp\left[-\frac{(\Delta\lambda - \Delta\lambda_1)^2}{\Delta\lambda_0^2}\right],$$

where $\Delta\lambda_0$ is the line broadening parameter and $\Delta\lambda_1$, the Doppler shift of the cloud.

If we assume that the absorbing feature is optically thin and its source function very low, we can deduce $\Delta\lambda_1$ directly, $\Delta\lambda_1$ represents the distance between the centers of the

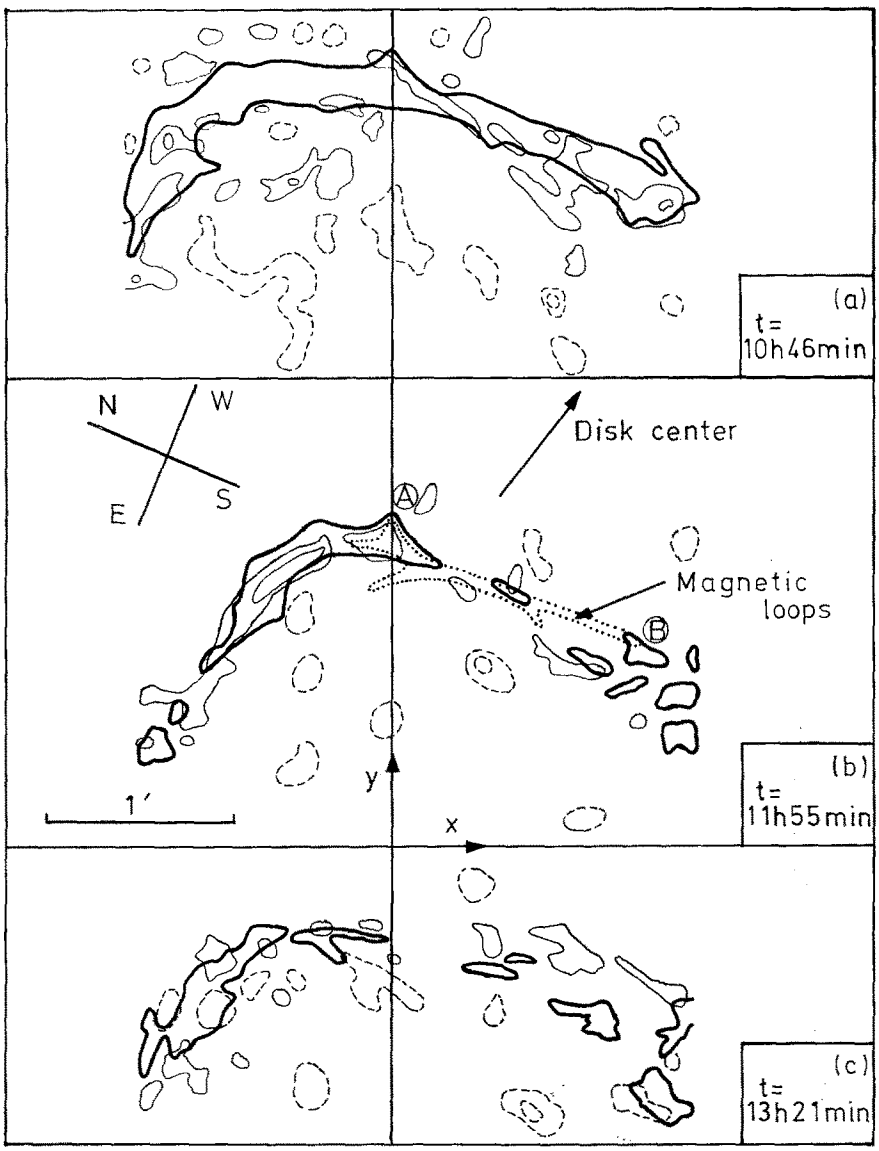

Fig. 2. Isocontours of Hα ± 0.3 Å intensities (thick line) of the filament and Doppler shifts (blue shift = thin line; red shift = dashed line). Velocity levels are ±1, ±4 km s^{-1}. (a) 10 hr 46 min UT; (b) 11 hr 55 min UT; (c) 13 hr 21 min UT.

$I_0(\lambda)$ profile and of $C(\lambda)$ (see Figure 3). It gives an upper value of the radial velocity of the material ejecta.

3.2. Dynamics of material ejecta inside a magnetic loop during the DB

Using the preceding technique we obtain maps of intensity $\Delta I_{\Delta\lambda_1}$ (Figure 4), and radial velocity $V_r = c\Delta\lambda_1/\lambda$ of section (a). Small thin threads of high velocity are visible in the

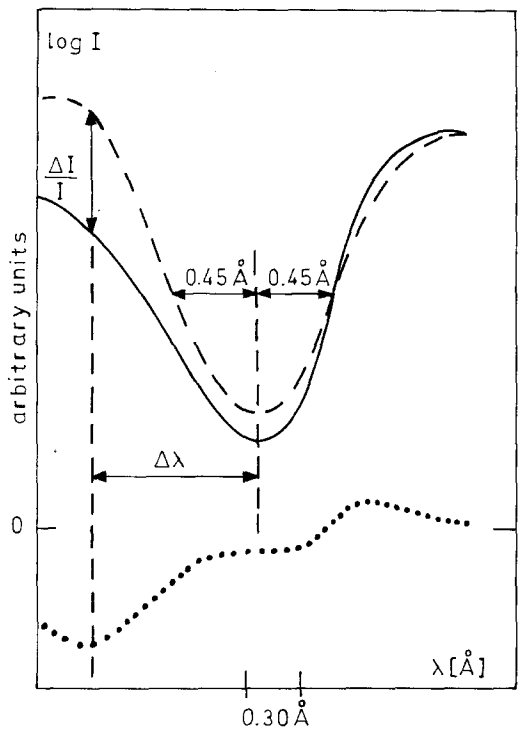

Fig. 3. 'Cloud model' interpretation of line profiles in the filament: mean chromospheric profile $I_0(\lambda)$, – – – –; observed current profile $I(\lambda)$, ———; $[I(\lambda) - I_0(\lambda)]/I_0(\lambda)$, · · · · · · . The intensity ΔI and velocity V_r of the cloud are derived.

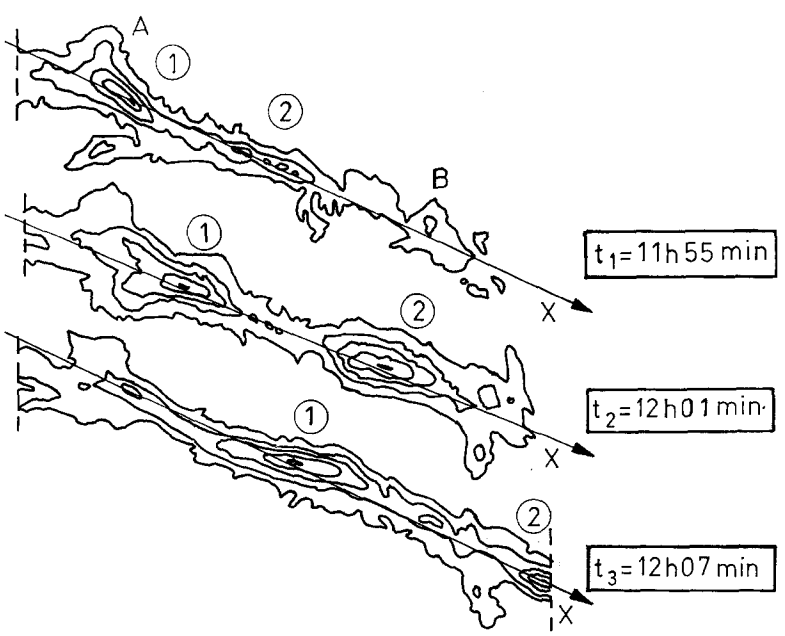

Fig. 4. 'Cloud model' intensity of the filament: *above*: 11 hr 55 min UT; *middle*: 12 hr 01 min UT; *below*: 12 hr 07 min UT. Two moving dark 'blobs' (denoted 1 and 2) are detected.

southern part (see Figure 2(b) where their contours are superposed between points A, B at time t = 11 hr 55 min). These fine structures can be considered as motions along a magnetic loop in a plane parallel to the line-of-sight. The motions have been studied during 12 mn with a time step of 1 mn. Only one foot of the loop (upward motions), point A in Figure 2(b), is visible on the MSDP field of view, the second one (downward motions) is outside of the field (section (b)) but is visible in the 3λ heliograph observations. Simultaneously type III bursts are observed at the same location suggesting a large velocity loop with particle acceleration. This loop, parallel to the filament seems to be closely related to its structure and support.

We present in Figure 4 the evolution versus time of the loop segment AB intensity. Two points of maximum absorption (denoted 1 and 2) can be considered as fluid particles and followed in the plane on the solar disk, giving the motions along the horizontal x-direction. Here we also notice the decreasing absorption of the filament at the location of the foot of the loop versus time (point A Figure 2(b)). It suggests a pumping of the filament material into the loop. Intensity and radial velocity cross sections at different times along the x-axis (Figure 5) allow us to calculate the velocity vector $V = (V_x, V_z)$ in the plane (x, z) of the loop (z being the vertical axis), using the heliographic coordinates of the filament to correct the radial and horizontal velocity

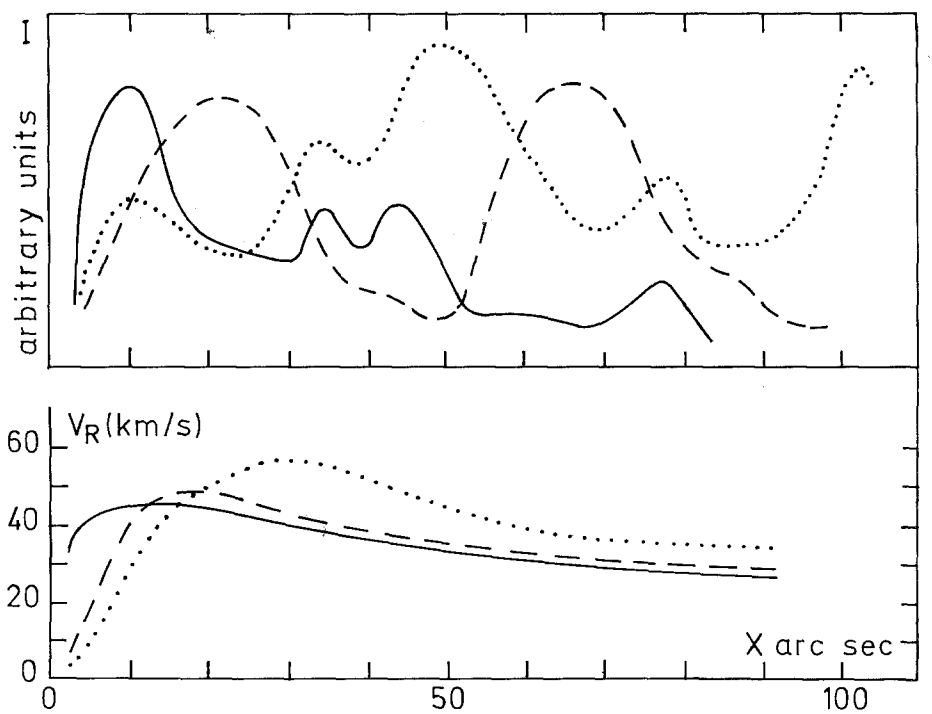

Fig. 5. Cross-sections of 'cloud model' intensity and velocity along the filament (x-direction); thick line: 11 hr 55 min UT; dashed line: 12 hr 01 min UT; dotted line: 12 hr 07 min UT.

components for the perspective effect. This result has been plotted in Figure 6(a–c) for particle 1.

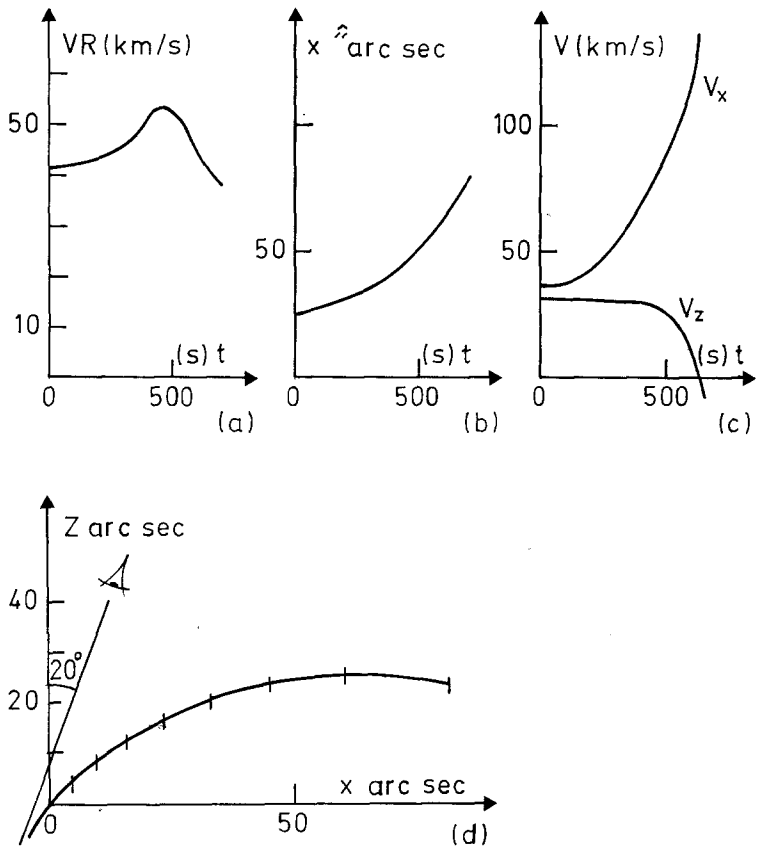

Fig. 6. Velocity vector and trajectory of the condensation (fluid particle): (a) radial velocity as a function of time; (b) location on the Sun as a function of time (proper motion); (c) velocity vector as a function of time; (d) trajectory.

From our knowledge of the vector **V** we deduce the trajectory of fluid particle 1 (Figure 6(d)). The top of the loop is higher than 25 000 km; highly supersonic velocities around 13 km s^{-1} are reached with strong acceleration near the foot ($-1.2g$, g being the solar gravity).

From the trajectory we deduce the variation of the vector **V** and of the altitude z of the fluid particle (prominence condensation) versus the curvilinear coordinates along the loop (Figure 7).

In order to understand the dynamics of the particle in the loop, we now investigate the acceleration provided by different mechanisms and driving forces, namely *stationary* siphon flows, then pressure or magnetic *pulses* at the base of a loop, and finally we consider the ejection of a magnetized plasma under the action of magnetic stresses in a diverging flux tube.

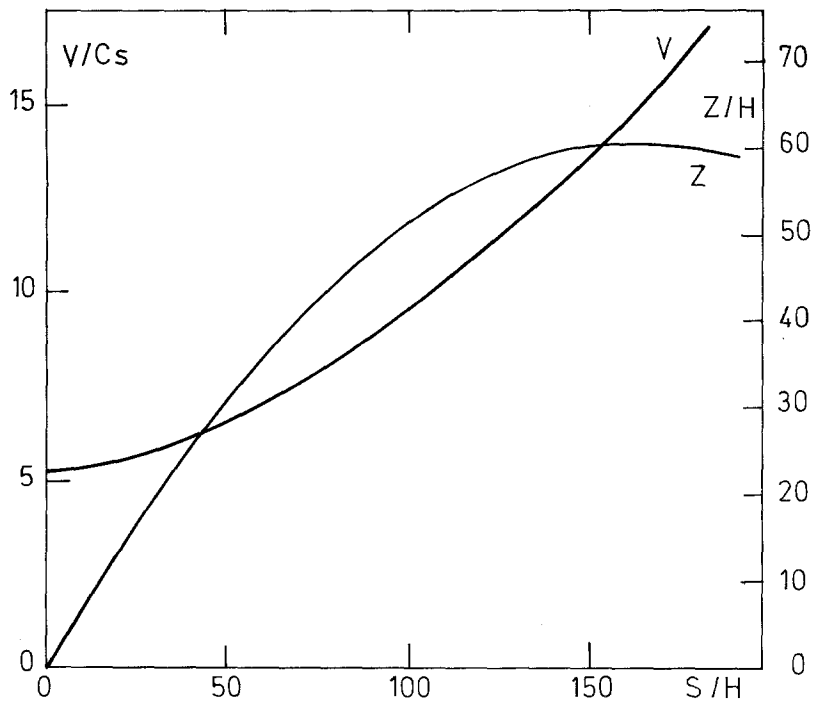

Fig. 7. Velocity and altitude of the condensation (fluid particle) as functions of the curvilinear abscissa s along the loop (trajectory). The velocity is normalized to the Hα sound speed, and the altitude to the Hα scale-height.

4. Mass Acceleration by Gas or Magnetic Pressure Pulse Mechanisms

4.1. Stationary siphon flow models

There is an extensive literature concerned with siphon flows in the context of mass motions in the solar atmosphere. Meyer and Schmidt (1968) discussed the Evershed motion as a siphon flow. Parker (1976) has considered the more complex situation of the dynamical equilibrium for flux tubes at photospheric levels where the magnetic field is given by radial pressure balance. Dynamical models of prominences based on the siphon mechanism have been proposed by Pikel'ner (1971), Ribes and Unno (1980), and Poland and Mariska (1986). The analysis of Cargill and Priest (1980) is also relevant. Here we will only consider the simplest models, our aim being to make direct comparisons with our observational results.

For isothermal steady flow we have the Bernoulli integral

$$\frac{V^2}{2} + \frac{kT}{m} \log\rho + gz = \text{const.},$$

where z is the altitude at a point along the flux tube. This may be rewritten as

$$\frac{\rho}{\rho_0} = e^{-z/H} e^{-(M^2 - M_0^2)/2},$$

where the subscript 0 refers to footpoint values. For a density scale height $H = c_s^2/g \simeq 300$ km, $z/H \simeq 100$, and with Mach numbers $M_0 < 1$, $M = 10$ (from observations), we can relate quantities between the top and bottom of the loop. Hence, $\rho/\rho_0 \simeq 10^{-65}$ and (from mass conservation) we would require a divergence in the cross-section σ of the loop, $\sigma/\sigma_0 \simeq 10^{64}$. This is not compatible with observation.

For adiabatic flow ($\gamma = \frac{5}{3}$) the Bernoulli integral is

$$\frac{V^2}{2} + \frac{\gamma}{\gamma - 1} \frac{P_0}{\rho_0} \left(\frac{\rho}{\rho_0}\right)^{\gamma - 1} + gz = \text{const.},$$

from which we obtain

$$\frac{\rho}{\rho_0} = \left[1 - \frac{\gamma - 1}{\gamma} \frac{z}{H} - \frac{M^2 - M_0^2}{2} (\gamma - 1)\right]^{1/\gamma - 1}.$$

This implies a *maximum height* z_m (given by $\rho = 0$) with an *upper limit* (given by $M = 0$). For example $z_m < 2.5H$ (with $M_0 = 0$) and $z_m < 3.33H$ (with $M_0 = 1$).

Clearly stationary isothermal or adiabatic flows cannot account for observations. Time dependent processes need to be investigated, as well as siphon flows including a full energy equation (with conduction, radiation, and heating). This last point will be the topic of a further paper. Now we focus on time-dependent mechanisms as the response of the atmosphere to a pressure or a magnetic pulse.

4.2. Pressure Pulse: An Order of Magnitude Model (The 'Pneumatic Spring')

We consider a simple model in which the dense blob of cool material (prominence condensation) is assumed initially to be in equilibrium and supported against gravity by the pressure of the photospheric layers at a point $s = s_0$, where s is the curvilinear coordinate along the loop (see Figure 8). The cross-section of the loop σ is assumed to be a constant. For the initial equilibrium we have

$$P_0 \sigma = mg \left(\frac{dz}{ds}\right)_0,$$

where m is the total mass of the blob and $(dz/ds)_0$ is the slope of the loop at the initial point $s = s_0$. Here we will neglect the coronal pressure above.

At time $t = 0$ the pressure P_0 is supposed to increase suddenly ($P_0 \rightarrow P_0'$) due to a local change of the boundary conditions (heating) in the photospheric layers. The blob will

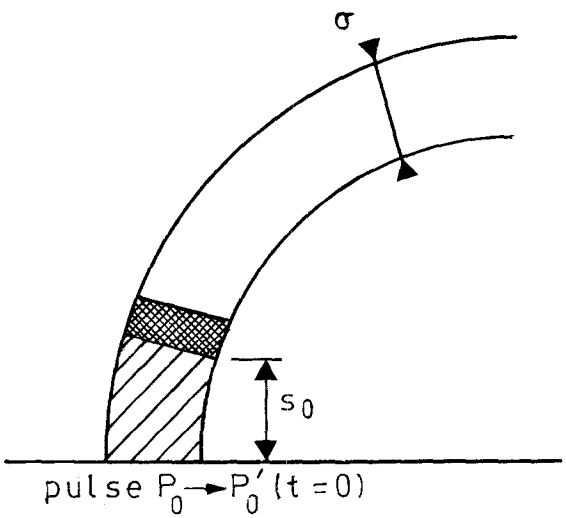

Fig. 8. A schematic picture of the gas pressure pulse mechanism in a loop.

begin to move and we may use the momentum equation

$$m \frac{d^2 s}{dt^2} = P\sigma - mg \frac{dz}{ds} .$$

As a specific example we will assume that the enhanced pressure P_0' occurs over one scale height, i.e., for $0 < s < H$ and that the blob is initially at $s_0 = H$. As the blob moves upward the volume $s\sigma$ occupied by the underlying hot material increases. For isothermal expansion we have $P = P_0' s_0/s$. Using the equilibrium condition for $P = P_0$ the momentum equation may now be rewritten as

$$m \frac{d^2 s}{dt^2} = \left\{ \frac{P_0'}{P_0} \frac{s_0}{s} \left(\frac{dz}{ds} \right)_0 - \frac{dz}{ds} \right\} mg .$$

Notice that for $s = s_0$, $P_0' = P_0$ (no pressure enhancement) we recover the equilibrium condition. The pressure enhancement P_0'/P_0 initially provides an acceleration which then decreases as the driving gas expands (s increases). We integrate this equation along the observed trajectory ($z(s)$ is known) for different values of the pressure enhancement P_0'/P_0 varying from 3 to 30, and with $s_0 = H$. The results are displayed in Figure 9. A strong pulse is necessary to accelerate the blob up to the loop summit. The form of the velocity curve disagrees with the observed case. From the computations the acceleration is strong at the foot point and diminishes along the loop. On the contrary, the observed acceleration is almost constant. We need to find another kind of mechanism to fit well the observations.

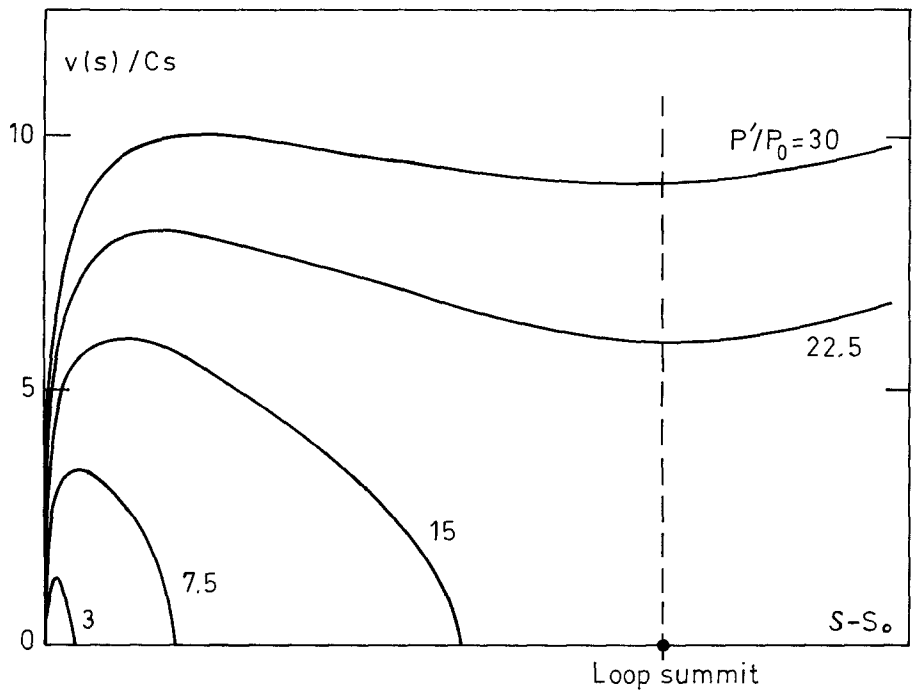

Fig. 9. Velocity as a function of the curvilinear abscissa s along the loop predicted by the gas pressure pulse mechanism ($\Delta P/P$ = 3, 7.5, 15, 22.5, and 30).

4.3. Mass acceleration by magnetic pulse in a constant cross-section tube ('the magnetic spring')

We investigate in this section the response of the atmosphere to a sudden twist at the foot point of a magnetic tube. We assume that, at time $t = 0$, the magnetic field at the foot point of the tube is twisted by angle ϕ. The condensation (blob) is assumed to be located between the region of uniform twist and the region of non-twisted field lines (see Figure 10). So the magnetic energy suddenly stored below the prominence condensation at the footpoint of field lines is converted to kinetic energy as the condensation moves outwards. The magnetic energy stored in a uniform twisted and force-free magnetic tube of constant cross-section, length L and radius R is given by

$$W = B_0^2 \frac{\pi L^3}{2\mu_0 \phi^2} \log\left(1 + \frac{R^2}{L^2}\phi^2\right) = \frac{\pi L}{\mu_0} \int_0^R B^2(r) r \, dr$$

with

$$\mathbf{B} = [0, B_\theta(r), B_z(r)]$$

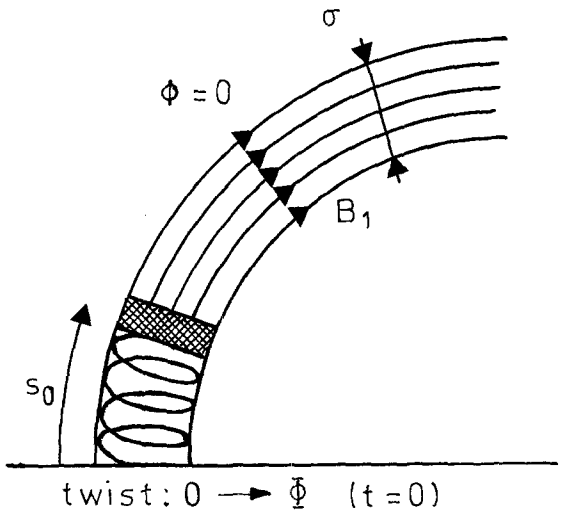

Fig. 10. A schematic picture of the magnetic pressure pulse mechanism in a loop.

and

$$B_\theta = B_0 \phi \frac{r}{L} \frac{1}{1 + \phi^2 r^2/L^2} ,$$

$$B_z = B_0/(1 + \phi^2 r^2/L^2) .$$

B_0 is the magnetic field along the axis of the loop.

We now assume that the magnetic field in the non-twisted part of the tube (above the condensation) is uniform and takes the value B_1. The conservation of the magnetic flux gives

$$B_0 = B_1 \frac{\phi^2 R^2}{L^2} \frac{1}{\log\left(1 + \frac{R^2\phi^2}{L^2}\right)}$$

and the magnetic energy stored in the non-twisted part, of length L', is

$$W' = \frac{B_1^2}{2\mu_0} \pi R^2 L' .$$

The driving force against gravity is then given by

$$F(s) = -\frac{\partial}{\partial s}(W + W')$$

$$= -\frac{\partial}{\partial s}\left\{\frac{B_1^2}{2\mu_0} \frac{\pi R^4}{s} \frac{\phi^2}{\log\left(1 + \frac{R^2\phi^2}{s^2}\right)}\right\} + \frac{B_1^2}{2\mu_0} \pi R^2 .$$

Using the same notation as in Section 4.2 ($\sigma = \pi R^2$) we obtain the equation of motion:

$$m \frac{\mathrm{d}^2 s}{\mathrm{d}t^2} = \frac{B_i^2}{2\mu_0} \sigma f(s) - mg \frac{\mathrm{d}z}{\mathrm{d}s},$$

where m is the mass of the condensation, and

$$f(s) = 1 + \frac{1}{\xi \log\left(1 + \frac{1}{\xi}\right)} \left\{ 1 - \frac{2}{(1+\xi)\log\left(1 + \frac{1}{\xi}\right)} \right\}$$

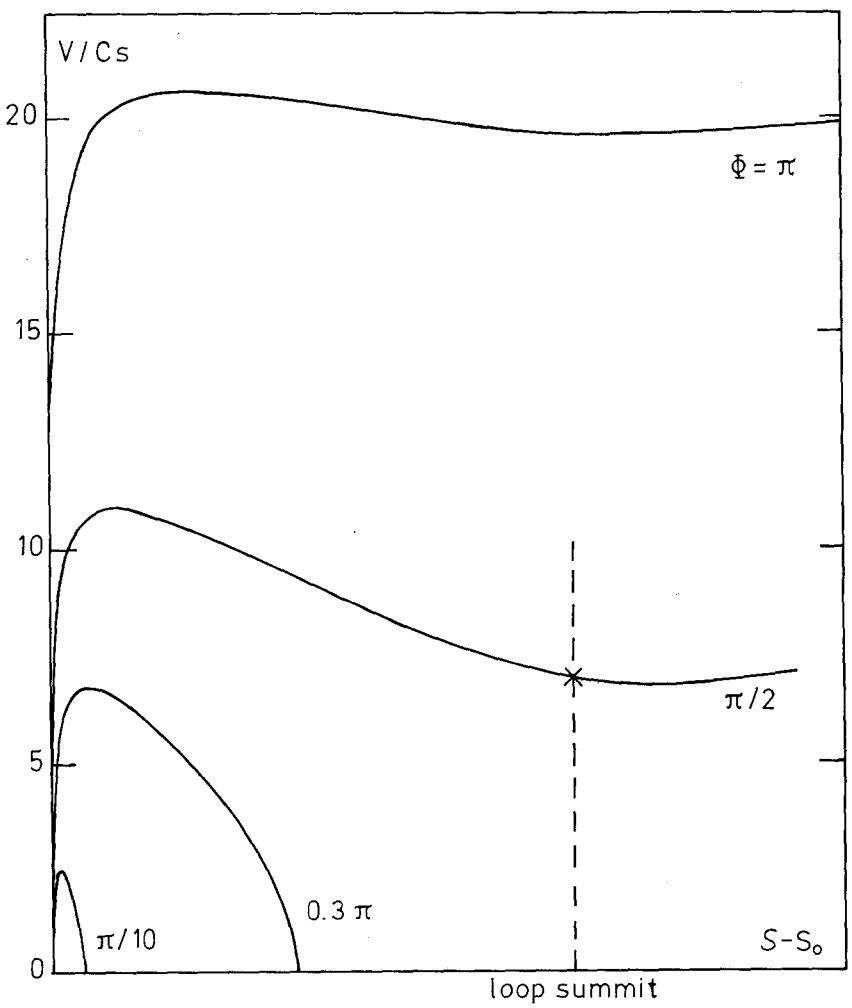

Fig. 11. Velocity as a function of the curvilinear abscissa s along the loop predicted by the magnetic pulse mechanism (twist $\phi = \pi/10$, 0.3π, $\pi/2$, and π).

with

$$\xi = \frac{s^2}{R^2\phi^2} ;$$

s_0 is the initial height of the twisted region. We integrate this equation along the observed trajectory ($z(s)$ is known) for different values of the twist ϕ. Results are displayed in Figure 11 for twists varying from $\pi/10$ to π. In this computation, we have taken $s_0 = H$. The results are comparable to those obtained with a pressure pulse: the behaviour of the velocity curve disagrees with the observed one, and clearly shows that it is necessary to investigate another kind of acceleration process.

5. Magnetic Acceleration of Plasmoïds

We now consider the behaviour of 'plasmoïds', magnetically isolated plasma clouds. Such clouds are acted on by forces due to the distortion of the ambient magnetic fields. Schlüter (1957) considered the simplest case namely that of a non-magnetized cloud moving through the coronal magnetic field. The material behaves as a diamagnetic body and is accelerated in the direction of decreasing magnetic field strength ('melon seed' mechanism). In this case the internal plasma pressure must on average balance the external magnetic and gas pressure. This means that the kinetic energy gained by the cloud is comparable to its thermal energy content and is consequently limited. Altschuler *et al.* (1968) proposed a surge mechanism based on numerical studies of the motion of plasma in the form of a vortex ring carrying a ring current. They found that in this case a (magnetized) plasma cloud may be expelled at the Alfvén velocity. The computed results were for an incompressible plasma. Pneuman (1983) has made a detailed analytical study of the motion of diamagnetic plasmoïds in the solar wind. The plasmoïds are modelled as cylindrical bodies with elliptical cross section and contain an internal magnetic field. The velocity of the solar wind is significantly increased if the effects of such diamagnetic plasmoïds are included. Dermendjiev (1984) has proposed an MHD-vortex as a model for solar photospheric bright points.

Useful information about the production, structure, and stability of plasmoïds is available from plasma experiments and fusion research on plasma confinement. The production of plasmoïds in the form of magnetized plasma rings has been studied in a series of experiments by Lindberg and Jacobsen (1964) and Alfvén and Lindberg (1975). Magnetically driven instabilities are observed which change the internal structure, but the lifetime of the plasma is nevertheless unexpectedly long. The spontaneous production of magnetized plasma rings is also seen in the plasma gun experiments of Turner (1970). Plasma rings have recently become of interest for fusion research as an example of a compact torus (CT) configuration. The classical spheromak solution discussed by Rosenbluth and Bussac (1979) will also be used here as a first approximation to the structure of a magnetized plasmoïd. They showed that for a fixed boundary the spheromak is marginally stable for all ideal MHD modes even implictly including tearing modes. Their treatment of surface and pressure driven modes is not immediately

applicable to the solar case where the plasmoïd is moving through the external coronal plasma. They found absolute stability for a slightly compressed structure (oblomak), but for a slightly elongated structure ('prolomak') a tilting instability appears tending to rotate the structure by 90° to a new stable configuration. Their results are extended by Finn and Manheimer (1981) and agree with the experiments of Jarboe *et al.* (1980). Rosenbluth and Bussac (1979), however, note that the tilting instability does not occur for reversed θ-pinches despite their elongated structure. Earlier Bartoli and Green (1963) argued, in the context of θ-pinch experiments, that an elongated cigar-shaped structure should be stable to tilting. Clearly there must be a strong dependence on external boundary conditions. In the solar case it may be argued that the magnetized coronal plasma, due to its inertia, provides a form of line tying. Simulation studies by Hayashi and Sato (1984) have shown that line-tying can stabilize spheromak tilting.

Having in mind the production of plasmoïds in theta-pinch experiments, it is interesting to reconsider the scenario proposed by Sturrock (1972) for surge flares and spicules. The basic idea is that during the emergence of magnetic flux, an individual flux tube may be hooked into the photosphere forming a coronal loop embedded in a more or less homogeneous field. At the re-entry point of the flux tube the magnetic polarity must be opposite to that of the surrounding photosphere as is often observed for surges (cf. Rust, 1968). Locally we then have a theta-pinch configuration with a roughly cylindrical current sheet separating regions of upward and downward magnetic fields. Sturrock argues for reconnection at a circular neutral line releasing flare-energy and leading to a surge ejection in the overlying fields. However, tearing modes would lead to current rings of the type observed in experiments, which could equally well be described as plasmoïds. If the original flux tube was twisted the resulting plasmoïds could well contain force-free fields of the type proposed in this paper.

Here we will now consider the motion of a spherical plasmoïd containing an internal magnetic field (Figure 12). This geometry in chosen for simplicity and in a real situation a non-spherical structure may be more stable. An essential feature of our model is that we will assume that the internal field is nearly force-free. The magnetic energy can then in principle greatly exceed the plasma thermal energy, allowing for acceleration to *highly supersonic* velocities even if the contained matter is at low prominence temperatures. This feature may be contrasted with the case of a non-magnetized plasmoïd which must contain high-temperature plasma in order to obtain large velocities.

In order to have a specific magnetic field configuration we follow Rosenbluth and Bussac (1979) and choose a constant-α force-free field where

$$\mathbf{j} = \alpha \mathbf{B} .$$

The spheroidal solutions, discussed for example by Lüst and Schlüter (1954), may be written in the form

$$\mathbf{B} = \mathrm{rot}\left(\frac{\psi \mathbf{e}_\varphi}{r \sin\theta}\right) + B_\varphi \mathbf{e}_\varphi ,$$

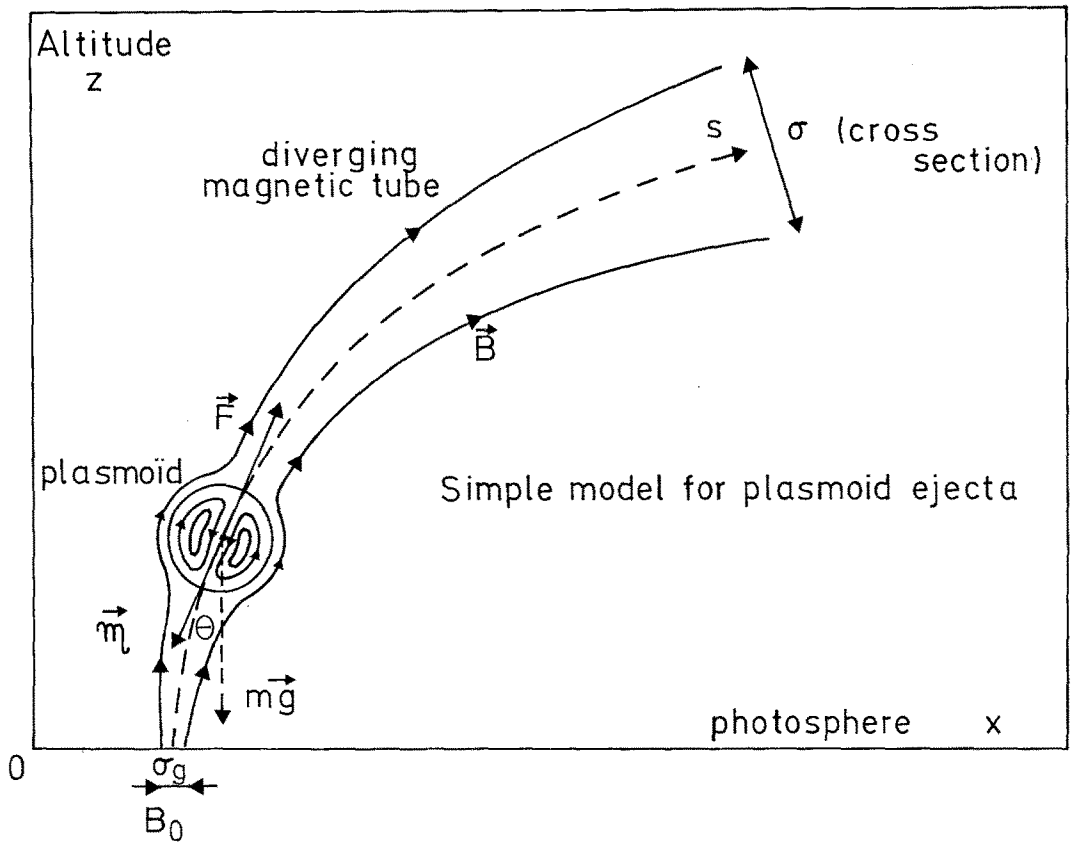

Fig. 12. A schematic picture of the acceleration mechanism of a magnetized plasmoïd in a loop.

where the poloidal flux function ψ is given by

$$\psi = \psi_\rho \left\{ \frac{\sin \alpha r}{\alpha r} - \cos \alpha r \right\} \sin^2 \theta$$

and the toroidal (azimuthal) field B_φ is then

$$B_\varphi = \frac{\alpha \psi}{r \sin \theta} .$$

We use this force-free solution inside the first spherical surface given by $\psi = 0$ so that the plasmoïd radius r_p is given by the first non-zero root of $\tan(\alpha r_p) = \alpha r_p$ (This ensures a simple toroidal topology. There are in fact infinitely many roots corresponding to nested sets of toroids). The ambient coronal magnetic field (for $r > r_p$) is to a first approximation taken to be uniform with a dipole distortion with, therefore, $B_\varphi = 0$ and

$$\psi = \psi_c \left\{ \frac{r^2}{r_p^2} - \frac{r_p}{r} \right\} \sin^2 \theta .$$

The dipole moment is $4\pi\psi_c r_p/\mu_0$.

Since we assume that pressure effects are small, any current layer on the $\psi = 0$ surface may be neglected and equilibrium requires that the magnetic field is continuous at $r = r_p$ so that

$$\psi_p = \frac{3\psi_c}{(\alpha r_p)\sin(\alpha r_p)} = \left\{\frac{3}{(\alpha r_p)\sin(\alpha r_p)}\right\}\frac{B_c r_p^2}{2},$$

where B_c is the uniform part of the external (i.e., coronal) field and we have used the condition $\psi(r_p) = 0$. For high electrical conductivity we may assume conservation of the internal poloidal and toroidal fluxes so that ψ = constant and $B_\phi r_p^2$ = const. for any given values of αr and θ (this follows automatically if ψ_p = constant). The force-free structure remains the same apart from a change of scale given by

$$r_p \sim B_c^{-1/2} \quad \text{and} \quad \alpha \sim B_c^{1/2}.$$

We note that the dipole moment is independent of the internal field structure:

$$\frac{4\pi\psi_c r_p}{\mu_0} = 2\pi r_p^3 \frac{B_c}{\mu_0}.$$

The argument we have presented can be generalised in a straightforward way for the case of an internal force-free field with α depending on the particular field line considered. A uniform expansion of the field leads to a similar structure with αr unchanged on corresponding field lines.

The net magnetic force on the plasmoïd may be found by integrating the Maxwell-stress over the surface, knowing the magnetic field at the surface. However, in the case we treat here of a spherical plasmoïd, the effect of the internal currents at the surface is equivalent to that of a dipole. In a non-uniform external field the force is then directly given by that on the equivalent dipole with a component along the field,

$$F = -2\pi r_p^3 \frac{\partial}{\partial s}\left(\frac{B_c^2}{2\mu_0}\right).$$

We rewrite this in the form

$$F = -\frac{3}{2} V B_c^{3/2} \frac{\partial}{\partial s}\left(2\frac{B_c^{1/2}}{\mu_0}\right),$$

where V is the plasmoïd volume. Flux conservation ($B_c r_p^2$ = const.) then implies that $VB_c^{3/2}$ is a constant. The equation of motion of the plasmoïd along the flux tube is, therefore,

$$m\ddot{s} = -\frac{3}{2} V_0 B_{c0}^{3/2} \frac{\partial}{\partial s}\left(2\frac{B_c^{1/2}}{\mu_0}\right) - mg\cos\theta,$$

with $v = \mathrm{d}s/\mathrm{d}t$ being the velocity; m is the plasmoïd mass and θ is the local angle of the flux tube from the vertical. V_0 and B_{c_0} are values at the initial point of the trajectory.

Integrating the equation of motion we find

$$v^2(s) = v^2(0) + \sigma v_{A_0}^2 \left[1 - \sqrt{\frac{B_c(s)}{B_{c_0}}} \right] - 2gz ,$$

where the Alfvén velocity v_{A_0} is given by

$$v_{A_0} = \frac{B_{c_0}}{\sqrt{\mu_0 \rho_0}}$$

and $\rho_0 = m/V_0$ is the average initial density of the plasmoïd. The magnetic field variation along the flux tube is related to the varying cross-section $\sigma(s)$ by

$$\frac{B_c(s)}{B_{c_0}} = \frac{\sigma_0}{\sigma(s)} .$$

We now have a simple algebraic equation *relating the velocity v of the plasmoïd to its position along the flux tube, given a varying cross-section* $\sigma(s)$.

To compare our model with the observations we use the above equation *to deduce the function* $B_c(s)/B_{c_0}$ given the velocity $v(s)$ and the trajectory $z(s)$. The only free parameter is the magnetic field B_{c_0} at the base of the loop (given ρ_0 this determines v_{A_0}). Figure 7 gives the velocity $V(s)$ deduced from observations. The implied variation of the magnetic field $B_c(s)$ is then given by Figure 13 for different values B_{c_0} at the base. The velocity is in units of the sound speed for prominence matter, $c_s \simeq 9.1$ km s^{-1} (for $T = 10^4$ K). The initial average density in the plasmoïd n_0 is taken to be 1.8×10^{17} m^{-3}. As the plasmoïd moves and expands spherically its density is proportional to $B_c^{3/2}$.

Since the free parameter is v_{A_0}, the initial Alfvén velocity, the curves are the same if new values of B_{c_0}, n_0 are taken such that $B_{c_0}^2 n_0^{-1}$ is the same.

For the plasmoïd to complete the observed motion, the initial field B_{c_0} must exceed a minimum value $\simeq 14.2$ G (implying $B = 0$ at the end of the trajectory). Thus, as may also be seen, an initial value $B_{c_0} = 10$ G is insufficient to account for the plasmoïd motion. As may be seen from Figure 13, $B_{c_0} = 20$ or 30 G are sufficient, the stronger field giving a weaker divergence of the flux tube. These field strengths are reasonable for the active region corona. At the end of the trajectory the plasmoïd density would be reduced to 8.4×10^{16} m^{-3} and 2.2×10^{16} m, respectively, in the two cases. These densities are acceptable for prominence material.

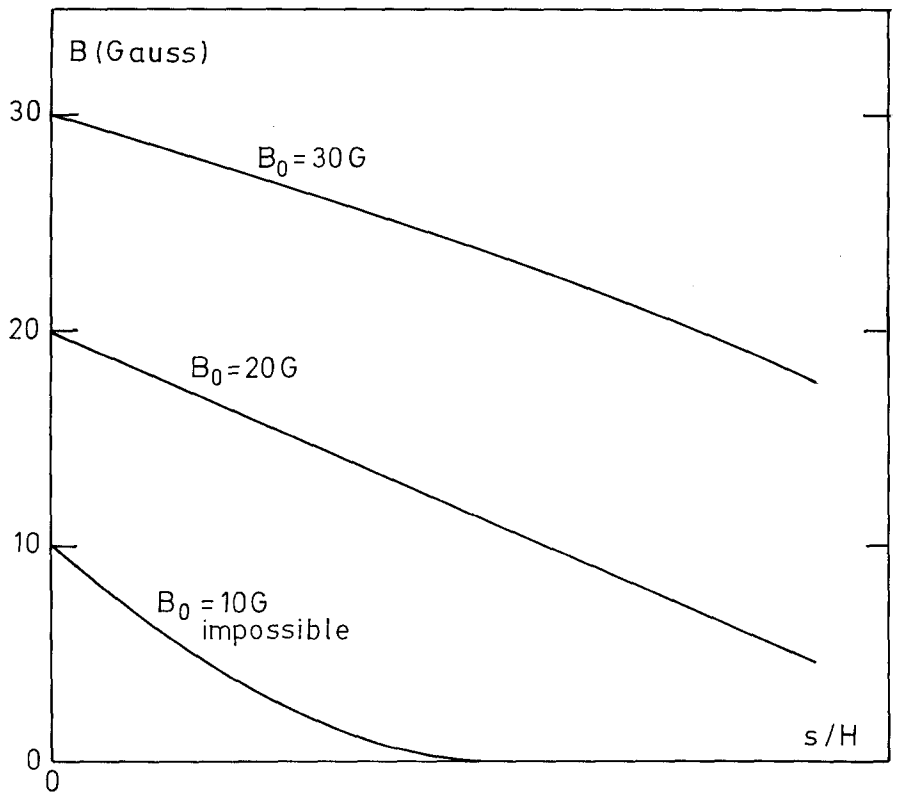

Fig. 13. Magnetic field as a function of the curvilinear abscissa s along the loop, predicted by the acceleration mechanism of a magnetized plasmoïd, using the observed velocities and trajectories of Figure 7.

6. Discussion and Conclusions

In two of the models we have looked at, the piston and the magnetic spring, energy is initially stored at the base of a flux tube (with constant cross section) in the form of thermal (pressure) and magnetic energy. The stored energy is converted to kinetic energy of the moving prominence condensation (blob) leading to a continuous decrease of the driving forces. This explains the similarity of the results. Both mechanisms give a strong initial acceleration at low altitude and the driving forces are localized to the foot of the magnetic arch.

In the case of the ejection of a plamoïd, magnetic energy is stored in the field of the moving plasmoïd; the energy release and the acceleration of the plasmoïd is determined by the variation of the cross section of the flux tube. This allows a continuous acceleration under the effects of magnetic stresses and the mechanism is therefore qualitatively different from the previous two.

Comparison with the observations during a DB analysed here suggest that the mechanism of the ejection of a magnetized plasmoïd in a divergent flux tube is the most probable explanation of the dynamics of the material ejecta.

Finally, we note again the importance of the internal approximately force-free field of the plasmoïd. Without this, the velocities obtained would be of the order of the sound speed of the contained matter.

References

Alfvén, H. and Lindberg, L.: 1975, *The Moon* **10**, 323.
Altschuler, M. D., Lilliequist, C. G., and Nakagawa, Y.: 1968, *Solar Phys.* **5**, 366.
Bartoli, C. and Green, T. S.: 1963, *Nuclear Fusion* **3**, 84.
Beckers, J. M.: 1964, Thesis, University Utrecht.
Cargill, P. J. and Priest, E. R.: 1980, *Solar Phys.* **65**, 251.
Dermendjiev, V. N.: 1984, in R. Muller (ed.), *High Resolution in Solar Physics*, Springer-Verlag, Berlin p. 236.
Dumas, G., Caroubalos, C., and Bougeret, J. L.: 1982, *Solar Phys.* **81**, 38.
Finn, J. M. and Manheimer, W. M.: 1981, *Phys. Fluids* **24**, 1336.
Hayashi, T. and Sato, T.: 1984, *Phys. Fluids* **27**, 778.
Jarboe, T. R., Henins, I., Hoida, H. W., Lindford, R. K., Marshall, J., Platts, D. A., and Sherwood, A. R.: 1980, *Phys. Rev. Letters* **45**, 1264.
Karpen, J. T., Oran, S. E., Mariska, J. T., Boris, J. P., and Brueckner, G. E.: 1982, *Astrophys. J.* **261**, 375.
Kleczek, J. and Kuperus, M.: 1969, *Solar Phys.* **6**, 72.
Konigl, A.: 1982, *Astrophys. J.* **261**, 115.
Kuperus, M. and Raadu, M. A.: 1974, *Astron. Astrophys.* **31**, 189.
Lindberg, L., and Jacobsen, C. T.: 1964, *Phys. Fluids* **7**, S44.
Lüst, R. and Schlüter, A.: 1954, *Z. Astrophys.* **34**, 263.
Malherbe, J. M., Simon, G., Mein, P., Mein, N., Schmieder, B., and Vial, J. C.: 1983a, *Adv. Space Res.* **2**, No. 11, 53.
Malherbe, J. M., Mein, P., and Schmieder, B.: 1983b, *Adv. Space Res.* **2**, No. 11, 57.
Mein, P.: 1977, *Solar Phys.* **54**, 45.
Meyer, F. and Schmidt, H. V.: 1968, *Z. Angew. Math. Mech.* **48**, 218.
Mouradian, Z., Martres, M. J., and Soru-Escaut, I.: 1986, in F. Moriyama and J. C. Hénoux (eds.), *Proceedings of the Japan–France Seminar on Solar Physics*, p. 195.
Parker, E. N.: 1976, *Astrophys. J.* **210**, 816.
Pikel'ner, S. B.: 1971, *Solar Phys.* **17**, 44.
Poland, A. I. and Mariska, J. T.: 1986, *Solar Phys.* **104**, 303.
Pneuman, G. W.: 1983, *Astrophys. J.* **265**, 468.
Priest, E. R. and Heyvaerts, J.: 1974, *Solar Phys.* **36**, 433.
Raadu, M. A.: 1979, in 'Physics of Solar Prominences', *IAU Coll.* **44**, 167.
Raadu, M. A. and Kuperus, M.: 1973, *Solar Phys.* **28**, 77.
Radioheliograph Group: 1980, *Solar Phys.* **88**, 385.
Ribes, E. and Unno, W.: 1980, *Astron. Astrophys.* **91**, 129.
Rosenbluth, M. N. and Bussac, M. N.: 1979, *Nuclear Fusion* **19**, 489.
Rust, D. M.: 1968, in K. O. Kiepenheuer (ed.), 'Structure and Development of Solar Active Regions', *IAU Symp.* **35**, 77.
Rust, D. M.: 1976, *Phil. Trans. Royal Soc. London* A. **281**, 427.
Schlüter, A.: 1957, in H. C. van de Hulst (ed.), 'Radio Astronomy', *IAU Symp.* **4**, 356.
Schmieder, B., Vial, J. C., Mein, P., and Tandberg-Hanssen, E.: 1983, *Astron. Astrophys.* **127**, 337.
Schmieder, B., Mein, P., Martres, M. J., and Tandberg-Hanssen, E.: 1984, *Solar Phys.* **94**, 133.
Simon, G., Mein, N., and Mein, P.: 1984, *Solar Phys.* **93**, 325.
Sturrock, P. .: 1972, in P. S. McIntosh and M. Dryer (eds.), *Solar Activity – Observations and Predictions*, MIT Press, Cambridge, U.S.A., p. 163.
Turner, R.: 1970, *Phys. Fluids* **13**, 2398.
Van Tend, W. and Kuperus, M.: 1978, *Solar Phys.* **59**, 115.